A Time Reversal-Based Acoustic Indoor Localization System at the Absolute Threshold of Hearing

Nadia Aloui, Kosai Raoof, Ammar Bouallegue, Stéphane Letourneur, and Sonia Zaibi

***Abstract*— We present in this paper an acoustic indoor location system that allows a simultaneous localization of sources with different location precisions. This is achieved by the use of the time reversal technique and the code-division multiple-access operation. The system was evaluated in terms of accuracy, precision, and location delay. Simulations and experiments were carried out while varying the number of sources and that of the precision levels. The effect of the signal-to-noise ratio on system performance was also studied. Results showed that our location system can achieve accuracy of 1.5 cm with 83% precision. Finally, we aimed to reduce the audibility of the location signal. An equalization filter based on the absolute threshold of hearing was applied to the emitted signal and a matched filter was introduced at the receiver. Results showed an improvement in location precision when compared with the location system without the equalization filter. A reduction in signal audibility was noted.**

***Index Terms*— Time reversal technique, different location precisions, simultaneous localization of sources, code-division multiple-access technique, absolute threshold of hearing.**

I. Introduction

INDOOR localization has recently attracted increasing attention owing to its interesting applications in everyday life. Application examples include security, healthcare, and tour guides.

Although the Global Positioning System (GPS) performs well outdoors, it fails indoors owing to the lack of a line of sight between the GPS receiver and satellites. Therefore, several location systems have been developed for use indoors. Most deploy triangulation and fingerprinting techniques.

Manuscript received June 18, 2015; accepted July 9, 2015. Date of publication July 28, 2015; date of current version September 14, 2015. This is an expanded paper from the International Conference on Indoor Positioning and Indoor Navigation 2013. The associate editor coordinating the review of this paper and approving it for publication was Prof. Janice Limson.

N. Aloui is with the GIPSA-Lab, UMR 5216 CNRS, University of Grenoble Alpes, 11, rue des Mathématiques, F-38402 Saint Martin d'Hères Cedex, France, and also with the Communication System Laboratory Sys'Com, National Engineering School of Tunis, University Tunis El Manar, Rommana 1068, Tunisia (e-mail: nadia.aloui@gipsa-lab.grenoble-inp.fr).

K. Raoof and S. Letourneur are with the Laboratoire d'Acoustique de l'Université du Maine Laboratory, University of Maine, Le Mans 72085, France (e-mail: kosai.raoof@univ-lemans.fr; stephane.letourneur@univ-lemans.fr).

A. Bouallegue and S. Zaibi are with the Communication System Laboratory Sys'Com, National Engineering School of Tunis, University Tunis El Manar, Rommana 1068, Tunisia (e-mail: ammar.bouallegue@enit.rnu.tn; sonia.zaibi@enit.rnu.tn).

Color versions of one or more of the figures in this paper are available online at http://ieeexplore.ieee.org.

Digital Object Identifier 10.1109/JSEN.2015.2459655

Triangulation-based location systems require a line of sight between emitters and receivers and estimate the target position according to distance or angle measurements. Generally, system components of known positions are fixed on the ceiling of a workspace to ensure visibility. The DOLPHIN system [1], the 3D-Locus [2], the Beep System [3], [4] and the location system presented in [5] are examples of triangulation-based systems. In indoor environments, although the fixed system components are placed on the ceiling, obstacles can block the visibility between the emitter and receiver.

Fingerprinting-based location systems do not require a line of sight. Target position estimation is based on premeasured data. The localization process is composed of two phases: an off-line phase and on-line phase. During the first phase, the positioning device is placed at predefined positions in the target environment where parameters that identify each position are extracted to define the signature of the target. During the second phase, the target signature is compared with signatures stored in the previously built database employing a positioning algorithm to estimate the target position. The ABS location system [6] is an example of a fingerprinting-based location system. It adopts an ambient sound-based signature and estimates the target position with room resolution employing a nearest-neighbor algorithm. Experimental results show that the system correctly locates the room with 69% precision.The SurroundSense system described in [7] combines ambient sound with light, color, acceleration and existing Wi-Fi based fingerprinting to build an identifiable fingerprint. The system can attain an average accuracy of 87% when considering 51 different stores. The location system presented in [8] and [9] adopts the time of arrival at the receiver of audible signals from emitters at known positions as a signature and estimates the target position through nonparametric kernel regression [10]. The system has accuracy better than 8.5 cm 80% of the time. Although the fingerprinting technique is suitable for indoor environments since it does not require a line of sight, it has drawbacks. Indeed, the database of premeasured data requires time to build and memory for storage. Moreover, the received signal strength, for most common fingerprints, is affected by reflection and scattering in indoor propagation. It is thus crucial to deploy techniques that are more robust for localization.

The time reversal technique is a focusing technique that benefits from the multiple paths. It reduces the channel to its

autocorrelation function, which resembles a Dirac function. This technique was developed in the field of ultrasound for many applications including the detection of defects in solids, underwater acoustics [11], medical imaging and ultrasound therapy. For some recent applications, time reversal has been used in the audible range [12] and for structural vibrations. The system presented in [13] deploys the time reversal technique to protect against underwater threats. It uses acoustic noise radiated by a hostile diver and focuses it back to the diver to disorient him/her. The signal is first recorded by the hydrophones of the time reversal acoustic system, then amplified, time-reversed and re-emitted simultaneously by the underwater transmitters. The emitted signals are focused on the hostile diver. Simulation results show that a time reversal acoustic system of 20 emitters 200 m distant from the diver and having peak acoustic power of 100 W is able to disorient and divert the diver away. In [14], the authors applied the time reversal method to localize the vibration sources in a complex structure. Transducers of a time reversal mirror are placed on the structure to record the vibration. The recorded signals are then time reversed and re-emitted by the time reversal mirror. The resulting vibration converges to the initial source. The authors have deployed ceramic patches having piezoelectric properties for the time reversal mirror. Therefore, because of their reversible effect, piezoelectric materials were used both as sensors to record the signals and as actuators to re-emit the time-reversed signals. A scanning is performed on 1 cm $\times$ 1 cm mesh using an accelerometer to cover surfaces of dimensions 4 cm $\times$ 15 cm and 18 cm $\times$ 6 cm. The vibration source was estimated as the position that presents the maximum vibration. A novel acoustic localization system was recently described [15]. The system is based on the time reversal technique and provides the location with different precisions. First, the user deploys a low-frequency signal to localize the destination, equipped with an acoustic source, in the whole area of interest with coarse precision. The user then switches to a high-frequency signal to estimate the destination position in a reduced area with fine precision. In this paper, we enrich the location system presented in [15]. Section II presents the time reversal technique and describes the spatial correlation diagram. Section III describes the location scenario of the multi-resolution location system and reports the results obtained in simulations and experiments. In section IV, we extend the multi-resolution location system to the multi-user and multi-source case and we evaluate its cumulative error distribution while varying the number of sources. Finally, in section V, we deal with signal audibility by employing psycho-acoustics. Finally, conclusions are given in section VI.

II. Time Reversal Technique

A. Principle

In acoustics, the wave propagation equation is invariant under time reversal in a heterogeneous and non-dissipative medium because it only involves even-order derivatives. This implies that, for any diverging wave $\psi(r_r, t)$, there is a corresponding wave $\psi(r_r, -t)$ converging to its acoustic source.

Cassereau and Fink developed the concept of the time reversal cavity [16]. They demonstrated, using the Helmoltz–Kirchoff theorem, that unique knowledge of the field on a closed surface suffices to accomplish the time reversal operation. It is then not necessary to know the field at every point of the considered volume to attain focalization. The time reversal cavity seems impractical. In fact, it requires a large number of transducers to cover the closed surface. In practice, it is replaced with a non-closed surface, called the time reversal mirror.

According to the reciprocity of the wave propagation equation and the Helmoltz–Kirchoff theorem, an experience of time reversal can be described in two phases: the emission phase and reception phase. During the first phase, a source emits, in the medium, an acoustic impulse that is reflected, diffracted and diffused. Transducers of the time reversal mirror then record the resulting wave. During the second phase, the received wave is re-emitted by every transducer but with inverse chronology. Cassereau and Fink demonstrated that the resulting wave is identical to the wave initially emitted but time reversed. This wave converges to the initial source. Moreover, they demonstrated that the size of the time-reversed focal spot, defined as the width at half height of the zone where energy is concentrated, is about half the source carrier wavelength.

B. Time Reversal Technique From a Signal Processing Point of View

Assuming linear time invariant systems, the received signal at position i can be written as the convolution of the signal $S_j(t)$ emitted by the source at position j and the channel impulse response $h_{ij}(t)$ between the source and receiver:

$$R_{ij}(t) = S_j(t) * h_{ij}(t). \tag{1}$$

We consider that each elementary source, i, of the mirror emits the signal that it received but with inverse chronology:

$$R_{ij}(-t) = S_j(-t) * h_{ij}(-t). \tag{2}$$

The received signal at a point m can therefore be written as:

$$Y_{mj}(t) = \sum_i S_j(-t) * h_{ij}(-t) * h'_{mi}(t). \tag{3}$$

$h'_{mi}(t)$ denotes the channel impulse response between i and m.

At the source position, we obtain [17]

$$Y_j(t) = \sum_i S_j(-t) * h_{ij}(-t) * h'_{ji}(t). \tag{4}$$

The time reversal is then considered a matched filter in the sense of signal processing. During the first phase of time reversal, the initially emitted signal is filtered by the propagation medium. Every spectral component of the impulse responses has a particular amplitude and phase. Time reversal does then nothing more than to return in the medium each impulse response without changing the relative amplitudes of the various frequency components so that they are exactly adapted to the environment, but while offsetting their phases so that they all arrive consistently at a point and at a given time.

Using the complex envelops $S_{e_j}(t)$, $h_{e_{ij}}(t)$ and $h'_{e_{mi}}(t)$ of signal $S_j(t)$ and the impulse responses $h_{ij}(t)$ and $h'_{mi}(t)$, the complex envelop of the received signal $Y_{mj}(t)$ can be written as

$$Y_{e_{mj}}(t) = \sum_i S^*_{e_j}(-t) * h^*_{e_{ij}}(-t) * h'_{e_{mi}}(t), \tag{5}$$

where a^* denotes the complex conjugate of a.

Given $h_{e_{ij}}(t) = \sum_k \alpha_{ij}^{(k)} e^{-jw\tau_{ij}^{(k)}} \delta(t - \tau_{ij}^{(k)})$ and $h'_{e_{mi}}(t) = \sum_l \gamma_{mi}^{(l)} e^{-jw\theta_{mi}^{(l)}} \delta(t - \theta_{mi}^{(l)})$, where $w = 2\pi f$ and f is in turn the carrier frequency, $\alpha_{ij}^{(k)}$ and $\tau_{ij}^{(k)}$ denote respectively the attenuation and delay of the path k between the source j and transducer i, and $\gamma_{mi}^{(l)}$ and $\theta_{mi}^{(l)}$ denote respectively the attenuation and delay of the path l between the transducer i and receiver m, equation (5) can be rewritten as

$$Y_{e_{mj}}(t) = \sum_i \sum_{l,k} \alpha^{*(k)}_{ij} \gamma^{(l)}_{mi} e^{jw(\tau_{ij}^{(k)} - \theta_{mi}^{(l)})} \times S^*_{e_j}(-t - \tau_{ij}^{(k)} + \theta_{mi}^{(l)}). \tag{6}$$

C. Correlation Diagram

The correlation diagram (or pattern directivity by analogy with physics) is given by $\zeta(m) = max_t\ (|Y_{e_{mj}}(t)|)$, where $S_{e_j}(t)$ is an impulse signal. When observing the expression of $Y_{e_{mj}}(t)$ given in equation (6), we note that the correlation diagram depends not only on the source and receiver positions relative to the transducer positions but also on the carrier frequency f.

Figure 1 shows the correlation diagrams of a source obtained with different values of frequency f. The diagram is computed at each point of an area having dimensions of 1.2 m × 1.2 m and centered at the source position. It is seen that the shape of the correlation diagram varies with f. In fact, the shape is controlled by the term $e^{jw(\tau_{ij}^{(k)} - \theta_{mi}^{(l)})}$ of equation (6). For a low frequency, this term changes slowly with the receiver position (traduced by the term $\theta_{mi}^{(l)}$), thus yielding a flat diagram. An increase in frequency produces pseudo-peaks and reduces the size of the peak at the source. For higher frequencies, the term varies rapidly, thus generating a sharp peak at the source position and pseudo-peaks around it.

III. Multi-Resolution Location System

We propose an acoustic location system that allows localization of a source with different precisions based on the time reversal technique. In particular, the system is based on the dependency of the correlation diagram on the source carrier frequency. Indeed, as described in subsection II-C, the peak at the source position widens as the frequency decreases. Hence, a higher frequency results in a sharper peak at the position of the source. The latter is then more accurately estimated at relatively high frequencies than at low frequencies.

The idea is to start the localization procedure at low frequency and then switch to a higher frequency while reducing the area of interest with the aim of being within the source peak. By doing so, we enhance the location precision achieved with the low frequency and we avoid the pseudo-peaks obtained with higher frequency that may be confused with the source position.

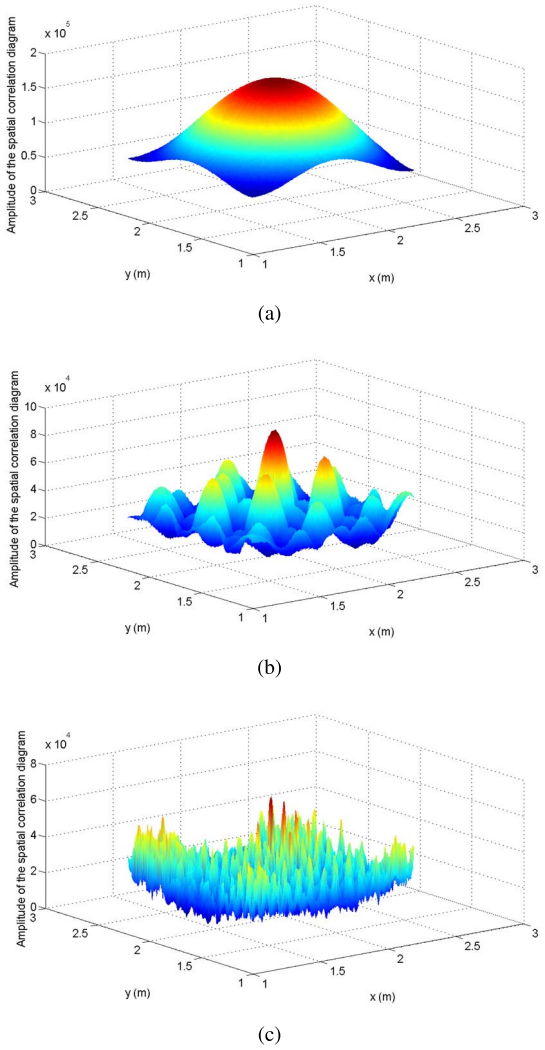

Fig. 1. Spatial correlation diagrams of the source placed at $(1.96m, 2.08m, 1.5m)$: (a) 200 Hz, (b) 800 Hz, (c) 4 kHz.

For validation of this concept, the localized source emits a Gold-code-modulated signal with M_f carrier frequencies. The receiver that searches for that source uses, first, a low frequency to attain or locate the source with coarse precision. It then switches to a higher frequency to search for the source in a reduced area, defined according to the previously estimated position, to determine the position of the source with finer precision. By doing so, a location is obtained with different precisions. The number of precision levels can be adjusted according to the desired application.

The system, as it is described, can be deployed in two ways. The first way is to estimate the position of a source wishing to be localized, and the second way is for a receiver to attain its destination equipped with a source.

A. Localization Scenario

The position of the source is estimated in the following steps.

1) The transducers of the time reversal mirror reverse and retransmit the signal coming from the source and modulated with M_f carrier frequencies.
2) The user unit demodulates the received signal using the lowest frequency.
3) The user unit then correlates the resulted signal with the time-reversed version of the source code.
4) The user unit computes the maximum value of that correlation. The user then moves in the area of interest using an optimization algorithm.
5) The process is repeated until the user finds the position that maximizes the correlation. This position corresponds to an estimate of the source position.
6) Once this is done, the user switches to a higher frequency and searches for the source position in a reduced area, defined according to the position estimated with lower frequency.

Different optimization algorithms can be used to guide the receiver to the source. Genetic algorithms iterate a population of solutions using a binary recombination operator called crossover and a unary neighborhood operator called mutation. The convergence of these algorithms is not easily regulated [18]. Simulated annealing is another general-purpose optimization procedure. Simulated annealing is inspired from annealing in metallurgy. It iterates a single solution using a neighborhood operator and employs a cooling schedule. This algorithm is adopted in the present study because it can be easily adapted to correlation diagrams (i.e., the diagram may or may not contain local optimums) by controling the value of one of its tuning parameters.

B. Simulated Annealing Algorithm

Simulated annealing [19] is a generic probabilistic metaheuristic random technique used to obtain global optimums for large optimization problems occurring in various areas including image processing, molecular chemistry and physics. Let S be a solution space and f be the cost function defined on members of S. Assume that the problem is to find a solution $i \in S$ that minimizes f over S. The simulated annealing starts with an initial solution that may be chosen at random. A neighborhood operator is applied to the current solution to generate a new solution. The change in cost is computed. If the cost is reduced, the generated neighbor is accepted and the current solution is rejected. If the cost is increased, the simulated annealing may accept the generated neighbor and reject the current solution though this generated solution degrades the cost function. By doing so, simulated annealing attempts to avoid locking in a local optimum. The acceptance or rejection of a bad solution is determined by a sequence of random numbers and with a controlled probability, which is called the acceptance function and is generally given as

$$exp(-\frac{\Delta f}{T}), \tag{7}$$

where Δf represents the change in f and T is a control parameter corresponding to temperature in analogy with physical annealing. The temperature plays an important role in the acceptance or rejection of the solution. Indeed, at high values of T, the acceptance function has high values and most solutions will be accepted. The algorithm visits a very large neighborhood of the current solution. At low values of T, the acceptance function has low values and most solutions will be rejected. The simulated annealing algorithm thus begins at a relatively high temperature to avoid locking in a local optimum. At each temperature, a certain number of solutions are generated. The temperature is gradually reduced.

TABLE I
PSEUDO-CODE OF AN ALGORITHM FOR THE SIMULATION OF ANNEALING [19]

Select an initial solution $S_i \in S$;
Select an initial temperature T
Set temperature change counter $t = 0$;
Repeat
Set repetition counter $n = 0$;
Repeat
Generate solution S_j, a neighbour of i;
Calculate $\Delta f = f(S_j) - f(S_i)$;
If $\Delta f \leq 0$ *then* $i := j$
else if $random(0,1) < exp(-\Delta f/T)$ *then*
$S_i := S_j$;
$n := n + 1$;
until $n = N(t)$;
$t := t + 1$;
$T := T(t)$;
until stopping criterion true.

Table I describes the simulated annealing algorithm in pseudo-code, where $T(t)$ is a temperature function that defines how the temperature is reduced and $N(t)$ represents the number of iterations defined at each value of temperature. $T(t)$ can be a proportional temperature function defined as

$$T(t+1) = \alpha\, T(t), \tag{8}$$

where α is a constant, typically lying between 0.8 and 0.99. The algorithm can be terminated either when the solution obtained at each temperature is unchanged during a number of consecutive temperature changes or after a fixed number of consecutive temperature changes, denoted by N_p.

Note that, for an initial value of $T = 0$, the simulated annealing algorithm acts as a gradient descent method. In this case, N_p is fixed to 1.

C. Evaluation of the System Performance

The system performance was evaluated in terms of accuracy, precision and location delay. The accuracy is defined as the highest tolerated error for a measure to be regarded as successful. The precision is the ratio of measurements with errors equal to or less than the accuracy. The location delay is evaluated as the average number of the receiver displacements that are required to localize or attain the source. This number includes not only the positions that optimize the correlation diagrams but also the positions that degrade it.

Our system variables were set as

- sampling frequency of 51200 Hz,
- carrier frequency of 200 Hz for the coarse range and
- length of a Gold code sequence of 127 chips.

TABLE II
TRANSDUCERS POSITIONS

Transducers	1	2	3	4
Positions (m, m, m)	(0.2; 2; 2)	(2; 0.2; 2)	(2; 3.8; 2)	(3.8; 2; 2)

Localization was performed in a room having dimensions of $4 \times 4 \times 2.2\ m^3$ and equipped with four transducers. Table II gives the exact positions of these transducers. The area in which a receiver begins to search for a source is within the focal spot. Its dimensions are proportional to half the lowest carrier frequency. Recall that the focal spot size is defined as the width at half-height of the zone where the energy is concentrated. In this study, we are rather interested in the area with almost no pseudo-peaks. In the following, the dimensions of the initial search area are set to $1.2 \times 1.2\ m^2$. The system, in this configuration, can be used jointly with another location system. Moreover, it can be deployed in indoor environments where objects are classified by their type. The evaluation of the system performance in wider spaces will require a lower carrier frequency.

In the following, we present the channel model that we adopted and the results that we obtained from simulations.

1) Simulations: We run simulations to evaluate the performance of our system. This explains why it was necessary to first define a channel model.

Channel Model: To model the acoustic reflections in an empty room, we adopted the channel model given by Allen and Berkley [20]. This model is based on an image technique and is given by

$$h_{ij}(t) = \sum_{p \in P} \sum_{m \in M} \beta_{x_1}^{m_x - q} \beta_{x_2}^{m_x} \beta_{y_1}^{m_y - j} \beta_{y_2}^{m_y} \beta_{z_1}^{m_z - q} \beta_{z_2}^{m_z} \frac{\delta(t - \tau)}{4\pi d} \tag{9}$$

for a source situated at j and a microphone at position i. (β_{x_1}, β_{x_2}, β_{y_1},β_{y_2}, β_{z_1}, β_{z_2}) are the reflection coefficients of the four walls, ceiling and floor. d is the distance between a source image and the microphone and τ is the delay of the corresponding reflected sound.

We chose a model of an empty room because it is difficult to model furniture or objects that may exist inside a room. Moreover, the time reversal technique is independent of the channel model because it reduces the channel to a Dirac delta function at the source position.

Results: For assessment of the system performance, we first restricted the system to two precision ranges: a coarse range obtained with a frequency of 200 Hz and a fine range obtained with a frequency of 4 kHz. This configuration is not the best and simply allows us to evaluate the performance of our localization system.

Localization was performed at 20 test positions. A receiver, situated at a random position, moves according to the simulated annealing algorithm to search for the position that maximizes the low-frequency correlation diagram (i.e., $f = 200$ Hz). It then switches to a frequency of 4 kHz to estimate the source position in a reduced area within

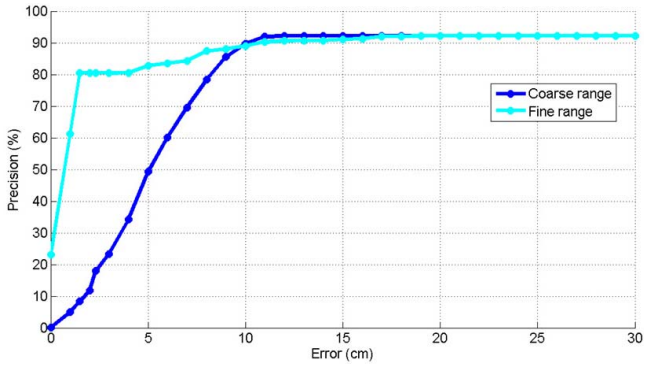

Fig. 2. Precision versus location estimation accuracy obtained with $M_f = 2$.

TABLE III
LOCATION DELAY

f	200 Hz	4 kHz
Average number of receiver displacements	22	121

fine precision. Figure 2 shows the precision obtained with both ranges. The system provides the location with accuracy of less than 10 cm in 89% of cases with the coarse range. With the fine range, the accuracy is better than 1.5 cm in 80% of cases. These results are obtained with an initial value of temperature $T = 0$, a displacement step $p = 6$ cm and a number of temperature cycles $N_p = 1$, for $f = 200$ Hz. These values are set empirically so as to obtain good precision. In the empirical setting, we varied one parameter and fixed all the remaining parameters. For $f = 4$ kHz, we did not adopt simulated annealing in the reduced area having dimensions of 16 cm $\times$16 cm, set in function of precision achieved with $f = 200$ Hz. In fact, in this case, simulated annealing would require us to begin with a high temperature to avoid the pseudo-peaks. Moreover, it would need a large value of N_p to converge to the global optimum (i.e., the peak at the source). There would thus be a large cost for the receiver to reach the source. Instead, the receiver scans the reduced area with a maximum step of 2 cm.

Table III reports that the average number of receiver displacements is almost 143. Hence, with two ranges, the receiver needs to move 143 times to localize the source with accuracy better than 1.5 cm in 80% of cases. This number is not negligible though it can be considered small when compared with the total number of possible receiver positions (i.e., the number of positions within the effective area). This is mainly due to the regular displacement of the receiver at $f = 4$ kHz in an investigated area having dimensions of $16 \times 16\ cm^2$ containing pseudo-peaks. Adding a new frequency between 200 Hz and 4 kHz could avoid these pseudo-peaks and reduce the area dimensions defined for the finest range (i.e., $f = 4$ kHz). Because the system provides good location precision for accuracy of 10 cm with $f = 200$ Hz, as shown in figure 2, we will set the dimensions of the reduced area in the intermediate range to twice 10 cm (i.e., 20 cm). If we consider the dimensions of the reduced area to be equal to the width of the focal spot for the intermediate frequency, the latter will be fixed at 800 Hz.

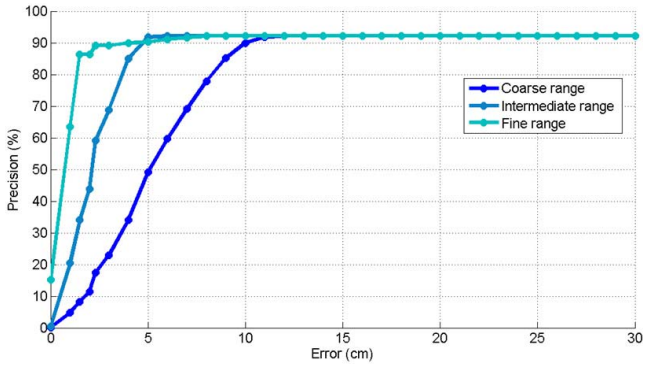

Fig. 3. Precision versus location estimation accuracy obtained with $M_f = 3$.

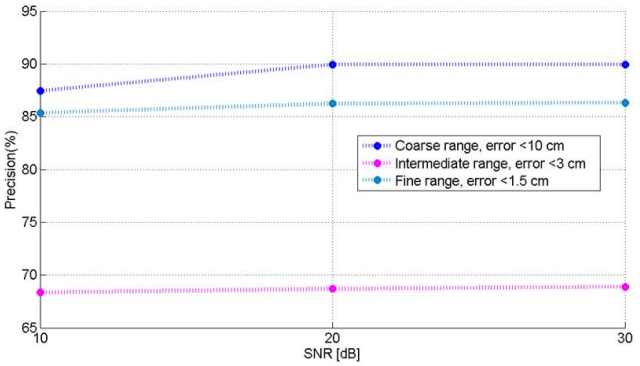

Fig. 4. Precision versus the SNR with $M_f = 3$.

Figure 3 shows the precision obtained with three ranges: a coarse range, intermediate range and fine range. Results are obtained with displacement steps of 6, 4 and 2 cm for frequencies of 200 Hz, 800 Hz and 4 kHz respectively and with area dimensions of 6 cm $\times$6 cm for $f = 4$ kHz, set in function of the precision obtained with $f = 800$ Hz. Note that the displacement step reduces as the frequency increases, since the width of the source peak (and thus the area dimensions) reduces with increasing frequency. Note also that the area dimensions for $f = 4$ kHz are proportional to the width of the relative focal spot.

As shown in figure 3, the system provides the location with accuracy of less than 10 cm in almost 89.9% of cases for the coarse range. For the intermediate range, accuracy better than 3 cm is achieved in almost 68.8% of cases. For the fine range, the system provides accuracy better than 1.5 cm with 86.2% precision. These performances are achieved with 70 receiver displacements. We consider that we have obtained a good compromise between the location delay and location accuracy.

To make a more complete evaluation of our system, we ran simulations while fixing the number of ranges to 3 and varying the values of the signal-to-noise ratio (SNR). Figure 4 shows the precision achieved with SNR values of 10 dB and 20 dB computed at the source position. Results extracted from figure 3 obtained with an SNR of 30 dB are also plotted. For an SNR of 10 dB, accuracy better than 10 cm is achieved in 87.4% of cases with the coarse range. With the intermediate range, the system provides the location with accuracy better than 3 cm in almost 68.3% of cases. With the fine range, the accuracy is better than 1.5 cm in 85% of cases. For SNR values of 20 and 30 dB, the system provides the location with accuracy of less than 10 cm in 89.9% of cases with the coarse range. Accuracy better than 3 cm with 68.8% precision is achieved with the intermediate range and accuracy better than 1.5 cm with 86.2% precision is achieved with the fine range. A maximum degradation in precision of 2.5% is then observed when comparing the case of 10 dB with the cases of 20 and 30 dB.

Fig. 5. Measurement environment.

In the following, we describe the experimental protocol that we adopted as well as the materials that we used in our experiments. Results are also presented.

2) Experiments: To validate simulation results obtained for two ranges, we conducted experiments in a practical training room at the National School of Engineering of Le Mans. The effective area, where we performed the experiment, measures $4 \times 4 \times 2.2\ m^3$ (figure 5). Localization with three ranges is considered hereafter.

Here, we aim to localize two sources in the effective area with two ranges, considering that the obtained results can be extrapolated to other sources in the effective area. The first source, denoted s_1, is situated at the center of the effective area (i.e., (2 m, 2 m, 1.52 m)) and the second, denoted s_2, is positioned at (2.5 m, 1.5 m, 1.52 m). Moreover, we acquired the received signal, after time reversal, at each position in an area having width $d = 48\ cm$ centered at the source position, with steps of 2 cm. A total of 625 measurements were thus made for each source. The measurement area is shown in figure 6.

It is important to note that it was not possible to keep the same number of localized sources, measuring step and width d as in simulations. In fact, an area having dimensions of 1.2 m $\times$ 1.2 m requires $14,641$ measurement points per source position. For 20 sources, we would have to make $292,820$ measurements. This would be possible if the microphone was mounted on a mobile support. However, in our experimentation, we manually displaced the microphone to measure step by step the time reversed signal in the effective area.

Experimental Protocol: To conduct our experiments, we followed the protocol described in [12] that takes advantage of the spatial reciprocity to create an initial virtual source. Recall that a classic experiment of the time reversal method

Fig. 6. Measurement area.

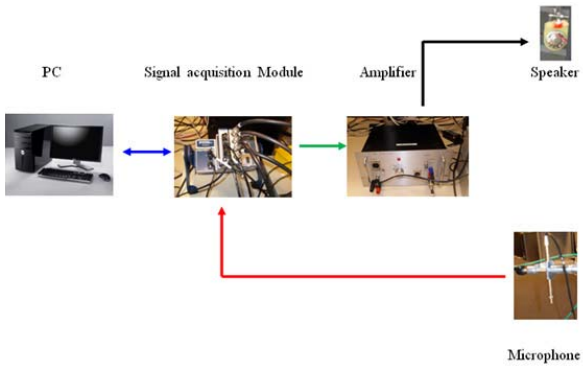

Fig. 7. Materials.

requires an initial source that emits an acoustic signal in the medium. The emitted signal is received by the microphones of the time reversal mirror and is then time reversed. The resulting signals are then re-emitted by the speakers of the mirror. In our experiments, we do not emit a sound with an initial source located at position j and record the field simultaneously with the microphones of the time reversal mirror. Instead, the same signal is successively transmitted by each speaker of the time reversal mirror, and recorded by the microphone placed at j, the position of the real source. The recorded signals are time reversed and then emitted simultaneously by the mirror speakers.

Material: Our experiments required four speakers, one microphone, a signal acquisition module, two amplifiers and a personal computer (figure 7). The signal acquisition module is composed of two modules: the NI9234 and NI9263. The former has four analog input channels, each having a delta–sigma analog-to-digital converter with resolution of 24 bits. The maximum data rate range is 51.2 Kech/s. The second module has four analog output channels, each having a string digital-to-analog converter with resolution of 16 bits. The microphone is $1/4$ diameter with an integral preamplifier and a dynamic range up to 122 dB. Its sensitivity is about 10 mV/Pa. The deployed speakers, model SC8N (8 ohm), have an almost flat frequency response from 20 Hz to 20 kHz [21] and the deployed amplifiers, model WI640, have an SNR of 100 dB and a bandwidth from 20 Hz to 20 kHz.

Data acquisition between the personal computer and the signal acquisition module is achieved using Lab VIEW and the signal processing is carried out using MATLAB.

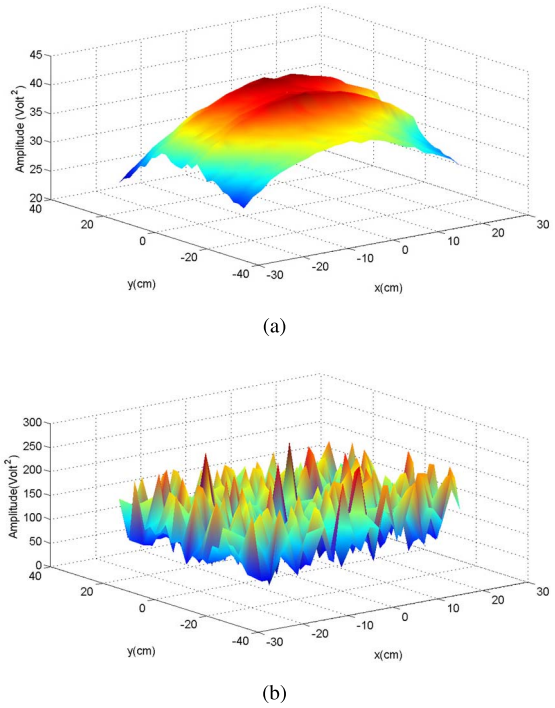

Fig. 8. Spatial correlation diagrams of the source s_1: (a) 200 Hz and (b) 4 kHz.

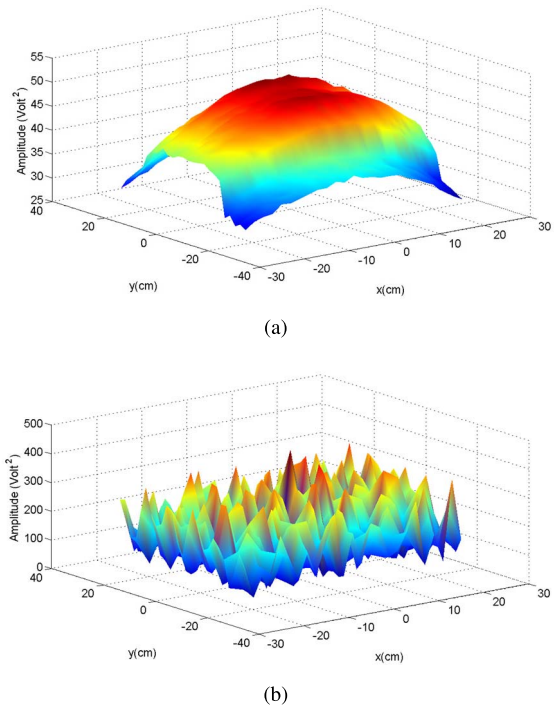

Fig. 9. Spatial correlation diagrams of the source s_2: (a) 200 Hz and (b) 4 kHz.

Results: Figures 8 and 9 show the correlation diagrams of the sources obtained with $f = 200$ Hz and $f = 4$ kHz. Table IV gives the precision per position for an error of $\simeq$0 cm obtained with $T = 0.1$, a step displacement $p = 2$ cm (equal to the measurement step), a reduced area having dimensions 16 cm $\times$ 16 cm and different values of temperature cycles N_p. For $f = 200$ Hz, the diagram is flat. For $f = 4$ kHz,

TABLE IV
PRECISION FOR AN ERROR OF $\simeq 0$ cm

N_p	1	2	4	6	8
Source s_1	98.4%	99.6%	100%	100%	100%
Source s_2	76%	84%	86.4%	90.6%	95.8%

there is a sharp peak at the source position and pseudo-peaks around it. The proposed system provides good location precision for both sources. With $N_p = 4$, the system localizes the sources s_1 and s_2 with error of $\simeq 0$ cm for 100% and 86.40% of measurements, respectively. These results confirm those obtained in simulations.

Next, we present our multi-resolution and multi-source location system.

IV. Multi-Resolution and Multi-Source Location System

At a given time, the multi-resolution location system allows only one user to locate or attain its desired destination. When there are several users, it is necessary to afford the location service to all users at the same time. To extend our system to the case of several users, we deployed the code-division multiple-access technique. This technique allows the discrimination between signals of different sources according to the direct sequence spread spectrum. A unique code is assigned to each source. A user that would like to attain destination j identified by source j and a code S_j demodulates, via its receiving unit, the received signal and correlates it with the code of source j. At the same time, a user that wishes to attain destination i ($i \neq j$) identified by source i and code S_i demodulates, via its receiving unit, the received signal and correlates it with the code of source i. Users then switch to a higher frequency to locate the sources with finer precision. Different spread spectrum sequences have been developed in the literature; e.g., m-sequences, orthogonal codes, and Gold codes. The latter are the most suitable for our system. In fact, despite the good auto-correlation and cross-correlation properties of m-sequences, there are few m-sequences because they are generated by primitive polynomials. Orthogonal codes are suited to perfectly synchronized systems. Indeed, they do not have good auto-correlation properties and their cross-correlation is equal to zero only when there is no lag between codes. Gold codes have good auto-correlation and cross-correlation properties. Moreover, they are generated in large numbers.

A. Formalism

To explain the principle of our system, we restrict the system to the case of N sources that simultaneously emit signals modulated with one frequency (i.e., $M_f = 1$). Denoting by $S_j(t)$ the code emitted by a source at position j, the received signal, $R_{e_i}(t)$, at the transducer situated at position i is given by

$$R_{e_i}(t) = \sum_{j=1}^{N} R_{e_{ij}}(t), \tag{10}$$

where

$$R_{e_{ij}}(t) = S_{e_j}(t) * h_{e_{ij}}(t). \tag{11}$$

$h_{e_{ij}}(t) = \sum_k \alpha_{ij}^{(k)} e^{-j w \tau_{ij}^{(k)}} \delta(t - \tau_{ij}^{(k)})$ is the complex envelop of the channel between the source j and transducer i. $\alpha_{ij}^{(k)}$ and $\tau_{ij}^{(k)}$ denote respectively the attenuation and delay of the k-th path between source j and transducer i.

After time reversal, the received signal at position m is given by

$$Y_{e_m}(t) = \sum_{j=1}^{N} Y_{e_{mj}}(t), \tag{12}$$

where

$$Y_{e_{mj}}(t) = \sum_i S_{e_j}^*(-t) * h_{e_{ij}}^*(-t) * h'_{e_{mi}}(t), \tag{13}$$

$$Y_{e_m}(t) = \sum_{j=1}^{N} \sum_i S_{e_j}^*(-t) * h_{e_{ij}}^*(-t) * h'_{e_{mi}}(t), \tag{14}$$

where $h'_{e_{mi}}(t) = \sum_l \gamma_{mi}^{(l)} e^{-j w \theta_{mi}^{(l)}} \delta(t - \theta_{mi}^{(l)})$ is the complex envelop of the channel between the transducer i and the receiver situated at position m. $\gamma_{mi}^{(l)}$ and $\theta_{mi}^{(l)}$ denote respectively the attenuation and delay of the path l between the transducer i and receiver m.

Replacing $h'_{e_{mi}}(t)$ in equation (14) by its expression, we obtain

$$Y_{e_m}(t) = \sum_{j=1}^{N} \sum_i \sum_{l,k} \alpha_{ij}^{*(k)} \gamma_{mi}^{(l)} e^{j w (\tau_{ij}^{(k)} - \theta_{mi}^{(l)})} \times S_{e_j}^*(-t - \tau_{ij}^{(k)} + \theta_{mi}^{(l)}). \tag{15}$$

The resulting signal is then correlated with the time reversed version of the code $S_{j_0}(t)$ of source j_0 that the user would like to attain. Hence, we obtain

$$\begin{aligned} C_{Y_{e_m}, S_{j_0}}(t) &= \sum_i \sum_{l,k} \alpha_{i j_0}^{*(k)} \gamma_{mi}^{(l)} e^{j w (\tau_{i j_0}^{(k)} - \theta_{mi}^{(l)})} A_{S_{j_0}}(-t - \tau_{i j_0}^{(k)} + \theta_{mi}^{(l)}) \\ &+ \sum_i \sum_{j=1, j \neq j_0}^{N} \sum_{l,k} \alpha_{ij}^{*(k)} \gamma_{mi}^{(l)} e^{j w (\tau_{ij}^{(k)} - \theta_{mi}^{(l)})} I_{S_{j_0}, S_j}(-t - \tau_{ij}^{(k)} + \theta_{mi}^{(l)}). \end{aligned} \tag{16}$$

$A_{S_{j_0}}(t)$ is the auto-correlation function of code $S_{j_0}(t)$ and $I_{S_{j_0}, S_j}(t)$ is the inter-correlation function of code $S_{j_0}(t)$ and codes $(S_j(t))_{j \neq j_0, j \in [1,N]}$.

Two factors may degrade our system performance: multiple-access interference and the near–far effect. Multiple-access interference is caused by the cross-correlation properties of the source codes. The near–far effect corresponds to the difference in received power for the sources' signals. In fact, the auto-correlation peak of the weaker signal can be masked by the significant cross-correlation peaks relative to the other stronger signals. It is thus difficult for the receiver to detect the weaker signal.

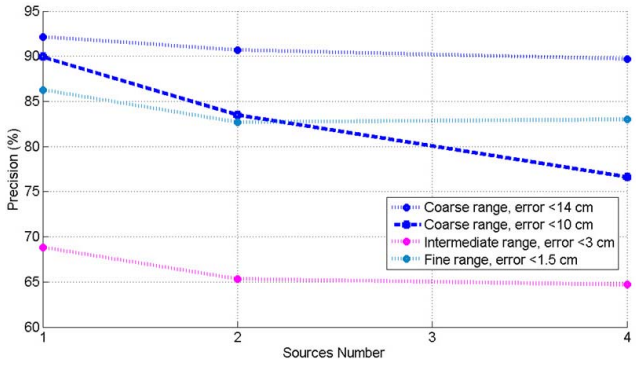

Fig. 10. Location precision obtained with $N \in \{1, 2, 4\}$.

B. Localization Scenario

The location scenario for $N > 1$ is similar to that presented in subsection III-A for $N = 1$, except for steps 1 and 3. The scenario becomes the following.

1) The transducers of the time reversal mirror re-emit simultaneously the reversed versions of the signals coming from N sources.
2) The user unit demodulates the received signal using the lowest frequency.
3) The resulting signal is then correlated against the time reversed version of the code of the source that the user wants to attain or localize.
4) The maximum value of that correlation is computed. The user then moves in the area of interest using the simulated annealing algorithm.
5) The process is repeated until the user finds the position that maximizes the correlation. This position corresponds to an estimate of the source position.
6) Once this is done, the user switches to a higher frequency and searches for the source position in a reduced area, defined according to the position estimated with lower frequency.

C. Evaluation of the System Performance

To evaluate the system performance, simulations were carried out and experiments were conducted. For simulations, we adopted the channel model presented in subsection III-C1. For experiments, the same materials described in subsection III-C2 were employed.

1) Simulations: Localization was performed at 20 test locations for a source number $N \in \{2, 4\}$ using three frequencies: 200 Hz, 800 Hz and 4 kHz. The distance between two neighboring sources is set to 30 cm. As the multi-resolution location system, the receiver begins to search for the source position in an area within the focal spot having dimensions of 1.2 m $\times$ 1.2 m. It switches then to higher frequency to estimate the source position in a reduced area within finer precision. Figure 10 shows the results obtained with different location ranges for $N \in \{2, 4\}$. The average precision for $N = 1$ is also reported.

As expected, the degradation in precision, with respect to $N = 1$, increases as the value of N grows. For the coarse range, the degradation in precision for accuracy below 10 cm changes from 6.5% to 13.3% as N varies from 2 to 4. This degradation is less in the intermediate range, being about 3% for $N = 2$ and 4% for $N = 4$. This is explained by the fact that, for the coarse range, the precision for higher values of accuracies obtained with $N \in \{2, 4\}$ approaches the precision obtained with $N = 1$. Because the research area, in the intermediate range, is reduced to an area having dimensions of 20 cm $\times$ 20 cm, it contains not only estimates with an error below 10 cm but also estimates with an error below 14 cm ($\simeq \sqrt{2} \times 10$ cm). For accuracy less than 14 cm, the precision is about 92.14%, 90.68% and 89.71% for $N \in \{1, 2, 4\}$ respectively. With the fine range, the system provides accuracy of 1.5 cm in almost 83% of cases for $N \in \{2, 4\}$. A degradation in precision of 3% is then observed compared with the case for $N = 1$.

TABLE V
PRECISION VERSUS LOCATION ESTIMATION ACCURACY OBTAINED WITH A SEPARATION OF 10 cm BETWEEN TWO NEIGHBORING SOURCES, $N = 2$

Range	Coarse range	Intermediate range	Fine range
Error (cm)	10	3	1.5
Precision (%)	80.5	62.6	81.56

To test our location system for small distances, we choose to divide the distance between two neighboring sources by 3. The number of sources N is fixed to 2. Table V gives the precision obtained with different ranges when setting the distance between two neighbouring sources to 10 cm. With the coarse range, a degradation in precision of 3% for accuracy of 10 cm is observed. With the intermediate range, the degradation is about 2.5% for accuracy of 3 cm. With the fine range, the system with two neighboring sources separated by 10 cm provides the location with 1.5 cm accuracy in almost 81.5% of cases, about 1% lower than that achieved with the system with two neighboring sources separated by 30 cm.

Although the location precision obtained with the multi-resolution and multi-user system is worse than that provided by the multi-resolution system, the multi-user system performs well. Moreover, it requires less time for localization since the sources' signals are simultaneously emitted.

2) Experiments: We evaluate the performance of our system in experiments conducted in a meeting room at the National School of Engineering of Le Mans (figure 11). The objective of this experiment is to validate the results obtained in simulations on real signals, using the same simulation parameters, and to evaluate the system performance in a real environment noisier than that of the simulations. The case of the simultaneous localization of two sources separated by 30 cm is considered. The first source, s_1, is placed at (2 m, 2 m, 1.52 m) and the second, s_2, is placed at (1.9 m, 1.72 m, 1.52 m). We measured, with steps of 2 cm, the signal received after time reversal in an area having dimensions of 70 $\times$ 70 cm^2. This leads to 1296 measurements. The measurement area is shown in figure 12. As with the experiments presented above (subsubsection III-C2), it was not

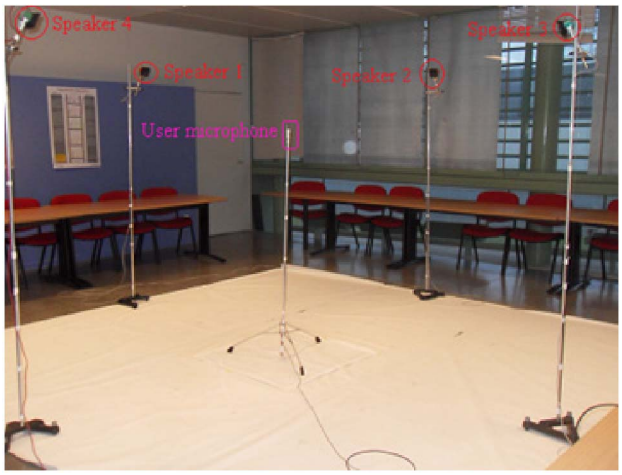

Fig. 11. Measurement environment.

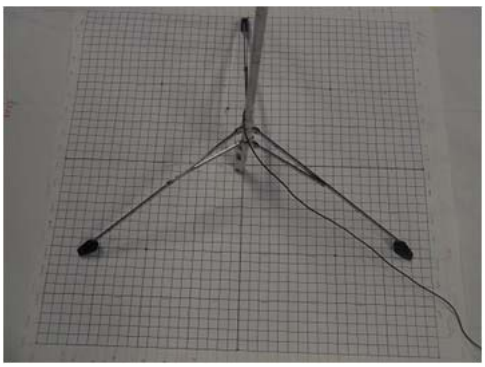

Fig. 12. Measurement area.

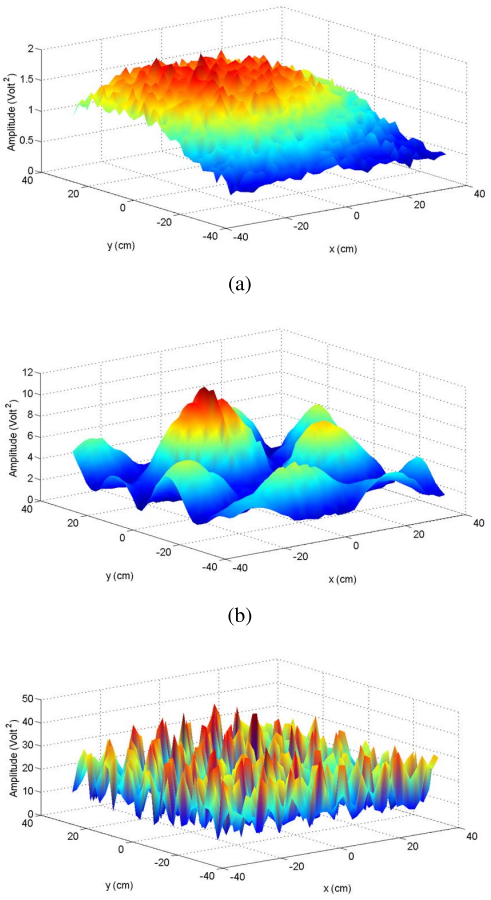

(a)

(b)

(c)

Fig. 13. Spatial correlation diagrams of the source s_1: (a) 200 Hz, (b) 800 Hz, and (c) 4 kHz.

possible to use the same dimensions of the measurement zone, the same number of source pairs and the same measurement step as in simulations. Indeed, this would require a large number of measurements that we could not make by varying the microphone position manually.

Experimental Protocol: As with the experiments described in subsection III-C2, the reciprocity theorem was applied to create two virtual sources at the positions of the real sources.

The experimental protocol is then as follows. During the first phase of the experiment, the signal relating to source s_1 is emitted successively by each speaker of the time reversal mirror, and then recorded by the microphone placed at the position of the real source s_1. The same process is repeated for source s_2: the speakers of the time reversal mirror emit successively the signal relating to source s_2. The signals are received by the microphone placed at the position of real source s_2. During the second phase, the signals resulting from both sources are summed at each transducer unit, time-reversed and then re-emitted simultaneously by the four speakers. Note that the process of the first phase is repeated for each of the two sources to respect the spatial reciprocity. The summation of the resulting signals during the second phase of the experiments guarantees a simultaneous localization of both sources.

Results: Figures 13 and 14 are spatial correlation diagrams of sources s_1 and s_2 and tables VI and VII give the precision obtained with different ranges. For the highest-frequency correlation diagrams, we observe a sharp peak at the source position and pseudo-peaks around it. For the intermediate range, the peak at the source becomes larger and there are fewer pseudo-peaks in the surroundings. For the coarse range, the diagram is almost flat—the spatial correlation amplitude varies slowly from one position to another—but we note some abrupt variations in amplitude in contrast with the correlation diagram obtained in simulations. This is explained by the fact that the experiment environment is noisier than the environment of the simulations. The variations can be reduced by increasing the length of the Gold code sequences since the autocorrelation peak value $A_{S_{j_0}}(0)$ increases linearly with the sequence length. This solution was adopted in [22], where barely audible signals were used for localization. Despite the noisy environment, the results reported in tables VI and VII show good location precision for both sources: accuracy better than 2 cm in 74% of measurements for source s_1 and accuracy better than ≈ 0 cm in 79% of measurements for source s_2.

It should be noted that, for example, the receiver can only use the coarse and intermediate ranges if it aims to locate the source with accuracy better than 8 cm. More generally, the receiver chooses the number of ranges of the location system depending on the desired precision (or the application).

The above results are obtained with an initial temperature $T = 0$ and a step displacement $p = 8$ and 4 cm for the coarse and intermediate ranges respectively. The dimensions of the

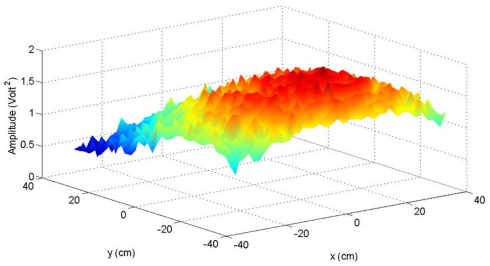

(a)

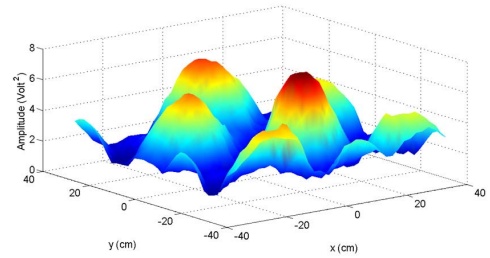

(b)

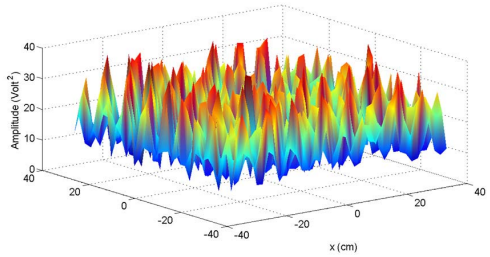

(c)

Fig. 14. Spatial correlation diagrams of the source s_2: (a) 200 Hz, (b) 800 Hz and (c) 4 kHz.

TABLE VI
PRECISION VERSUS LOCATION ESTIMATION ACCURACY FOR SOURCE s_1

Error (cm)	0	2	4	6	8	10
Coarse range (%)	0	11.40	13.40	20.40	31.80	43.20
Intermediate range (%)	14.60	45.20	60.60	67.20	74.00	77.40
Fine range (%)	0	74.00	74.00	74.00	74.00	74.60

TABLE VII
PRECISION VERSUS LOCATION ESTIMATION ACCURACY FOR SOURCE s_2

Error (cm)	0	2	4	6	8	10
Coarse range (%)	0	3.40	7.60	28.20	40.40	63
Intermediate range (%)	23.2	57.4	76.6	78	78.80	86.60
Fine range (%)	78.80	78.80	78.80	78.80	79.60	82.00

reduced area are set to 28 cm × 28 cm for the intermediate range. For the fine range, the receiver moves steadily with steps of 2 cm in an area having dimensions of 12 cm × 12 cm. These values differ from those used in the simulations because the simulation and experiment conditions are not identical.

V. SIGNAL AUDIBILITY

In the above analysis, our objective was to propose location solutions that allow simultaneous locating with different precisions. However, we did not address the limitation of using an audible sound for indoor localization. In practice, the transmission of an audible sound in an indoor environment might disturb people. In [22], the authors overcome this limitation by emitting a barely audible signal. To improve the SNR, they deployed signals of long duration. The authors also suggested combining the localization signal with music. The preliminary results showed that this slightly affects the performance of their location system.

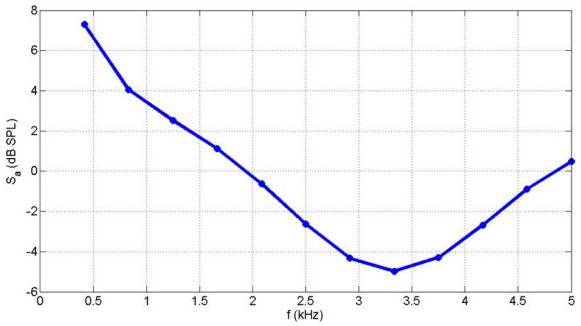

Fig. 15. Hearing absolute threshold.

Our solution for dealing with signal audibility is based on the absolute threshold of hearing. The latter defines the limit above which sound becomes audible. It is given by a nonlinear function,

$$S_a(f) = 3.64 \times f^{-0.8} - 6.5 \times exp(-0.6 \times (f - 3.3)^2) + 10^{-3} \times f^4 (dBSPL), \quad (17)$$

derived from the results of experiments conducted by Fletcher in a non-noisy environment, where f denotes the frequency in a unit of kilohertz.

Figure 15 shows the absolute threshold of hearing for $f \in [100Hz; 5kHz]$. It is noted that this threshold is higher for some frequency intervals than for others. Our idea is thus to send a signal having higher amplitude for frequencies at which the human ear is less sensitive. This is accomplished using an equalization filter based on the absolute threshold of hearing. To this end, the threshold is first converted to a linear scale according to

$$S_a(f) = 10 \times log_{10}((\frac{P_a}{P_{a_0}})^2), \quad (18)$$

where P_a represents the acoustic pressure and $P_{a_0} = 2 \times 10^{-5}$ Pa the reference pressure.

Applying an inverse Fourier transform to the resulting pressure, we obtain the impulse response of the filter, which we denote $h(t)$ (figure 16). At the receiver side, a matched filter $g(t)$ is used; the filter is defined as

$$g(t) = h(-t). \quad (19)$$

Because the location is estimated in the second phase of the time reversal operation and the first phase is controlled by the administrators of the location system, filter $h(t)$ is applied to the signals that are time reversed by the transducers of the time reversal mirror and filter $g(t)$ is applied to the signal received by the users of the system. The study conducts simulations considering the single-user case and using the

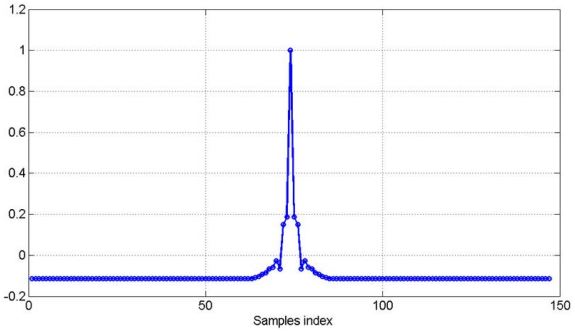

Fig. 16. Normalized impulse response of filter $h(t)$.

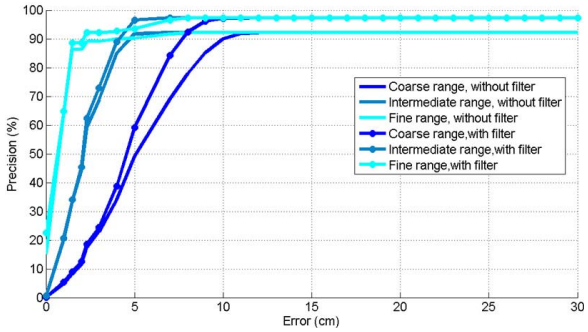

Fig. 17. Location precisions obtained with and without the equalization filter.

channel impulse response previously mentioned and the 20 test positions defined in subsubsection III-C1. Results are shown in figure 17. For comparison, we also report the performance of the system without the equalization filter.

At the coarse range, improvement in precision of about 7% for accuracy of 10 cm is observed compared with the system without the filter. The system with the filter provides about 4% better location precision for accuracy of 3 cm and 2% better location precision for accuracy of 1.5 cm at the intermediate and fine ranges, respectively. Moreover, for superior values of errors , the improvement in precision obtained by the use of the equalization filter $h(t)$ and the matched filter $g(t)$ is 5% for all ranges. The improvement in precision for the system with the equalization filter is mainly due to the maximization of the SNR resulting from the employment of a matched filter at the receiver. To investigate audibility, we played two versions of the signals emitted by the transducers—with and without the equalization filter—to six people whose ages ranged between 26 and 30 years and whose mean age was 28 years. The people noticed a reduction in the audibility of the filtered signal compared with that of the original signal.

VI. Conclusion

In this paper, we presented an acoustic localization system that is based on the time reversal technique and code-division multiple-access technique. The system allows a simultaneous localization of sources and permits the user to adjust the location precision for the desired application. Performance was first tested in simulations and then validated by experiments conducted at the National School of Engineering of Le Mans by varying the number of sources and the number of location precisions. Although the precision is reduced for a number of sources $N \in \{2, 4\}$ compared with the case for $N = 1$, the system still performs well, providing accuracy better than 1.5 cm in almost 83% of cases when the distance between two neighboring sources is set to 30 cm.

We are also interested in reducing the audibility of the location signal employing psycho-acoustics. An equalization filter based on the absolute threshold of hearing is used at the receiver side. Our results showed an improvement in precision of 5% when compared with the case of the location system without a filter. Moreover, we noted a reduction in the audibility of the filtered signal compared with that of the original signal.

Our system could be employed in a supermarket. The time reversal mirror would then be fixed on the ceiling, the localized sources on the discount items and the microphone of the user on a cart. The user moves with his or her cart to search for the sale items. The source signals could also be mixed with music played in the supermarket to allow localization in a less disturbing manner.

In this study, we evaluated our system performance assuming that the receiver has a priori information on the source position. The system, in this configuration, can be used jointly with other location systems. It can also be deployed in indoor environments where objects are classified by type or identification number. In future work, we aim to evaluate our system performance in a wider area. Hence, we should deploy a frequency value lower than 200 Hz to obtain a flat diagram that covers the whole zone of interest. Moreover, our work in this study focuses on localization in two dimensions. A three-dimensional localization will be studied in the near future.

References

[1] M. Hazas and A. Hopper, "Broadband ultrasonic location systems for improved indoor positioning," *IEEE Trans. Mobile Comput.*, vol. 5, no. 5, pp. 536–547, May 2006.

[2] J. C. Prieto *et al.*, "Performance evaluation of 3D-LOCUS advanced acoustic LPS," *IEEE Trans. Instrum. Meas.*, vol. 58, no. 8, pp. 2385–2395, Aug. 2009.

[3] C. V. Lopes, A. Haghighat, A. Mandal, T. Givargis, and P. Baldi, "Localization of off-the-shelf mobile devices using audible sound: Architectures, protocols and performance assessment," *ACM SIGMOBILE Mobile Comput. Commun. Rev.*, vol. 10, no. 2, pp. 38–50, Apr. 2006.

[4] A. Mandal, C. V. Lopes, T. Givargis, A. Haghighat, R. Jurdak, and P. Baldi, "Beep: 3D indoor positioning using audible sound," in *Proc. 2nd IEEE Consum. Commun. Netw. Conf.*, Jan. 2005, pp. 348–353.

[5] C. Sertatil, M. A. Altinkaya, and K. Raoof, "A novel acoustic indoor localization system employing CDMA," *Digit. Signal Process.*, vol. 22, no. 3, pp. 506–517, 2012.

[6] S. P. Tarzia, P. A. Dinda, R. P. Dick, and G. Memik, "Indoor localization without infrastructure using the acoustic background spectrum," in *Proc. 9th Int. Conf. Mobile Syst. Appl. Services (MobiSys)*, Bethesda, MD, USA, 2011, pp. 155–168.

[7] M. Azizyan, I. Constandache, and R. R. Choudhury, "SurroundSense: Mobile phone localization via ambience fingerprinting," in *Proc. 15th Annu. Int. Conf. MobiCom*, Beijing, China, 2009, pp. 261–272.

[8] N. Aloui, K. Raoof, A. Bouallegue, S. Letourneur, and S. Zaibi, "A novel indoor localization scheme based on fingerprinting technique and CDMA signals," in *Proc. Int. Conf. Indoor Positioning Indoor Navigat. (IPIN)*, Sydney, NSW, Australia, Nov. 2012, pp. 1–5.

[9] N. Aloui, K. Raoof, A. Bouallegue, S. Letourneur, and S. Zaibi, "Performance evaluation of an acoustic indoor localization system based on a fingerprinting technique," *EURASIP J. Adv. Signal Process.*, vol. 2014, p. 13, Jan. 2014.

[10] W. K. Härdle, M. Müller, S. Sperlich, and A. Werwatz, *Nonparametric and Semiparametric Models* (Springer Series in Statistics). Berlin, Germany: Springer-Verlag, 2004.

[11] H. C. Song, W. A. Kuperman, W. S. Hodgkiss, T. Akal, and C. Ferla, "Iterative time reversal in the ocean," *J. Acoust. Soc. Amer.*, vol. 105, no. 6, pp. 3176–3184, 1999.
[12] E. Bavu, "Le puits à retournement temporel dans le domaine audible: Un outil de focalisation et d'imagerie à haute résolution de sources sonores et vibratoires," Ph.D. dissertation, Sci. Mécaniques, Acoust. Électron., Univ. Pierre Marie Curie, Paris, France, Nov. 2008.
[13] A. Sutin and Y. Sinelnikov, "Time reversal acoustic approach for non-lethal swimmer deterrent," in *Proc. Int. Waterside Secur. Conf. (WSS)*, Nov. 2010, pp. 1–5.
[14] D. Vigoureux and J.-L. Guyader, "A simplified time reversal method used to localize vibrations sources in a complex structure," *Appl. Acoust.*, vol. 73, no. 5, pp. 491–496, 2012.
[15] N. Aloui, K. Raoof, A. Bouallegue, S. Letourneur, and S. Zaibi, "Multi-resolution localization method based on time reversal and simulated annealing algorithm," in *Proc. Int. Conf. Indoor Positioning Indoor Navigat. (IPIN)*, Montbéliard, France, Oct. 2013, pp. 1–9.
[16] D. Cassereau and M. Fink, "Time-reversal of ultrasonic fields. III. Theory of the closed time-reversal cavity," *IEEE Trans. Ultrason., Ferroelectr., Freq. Control*, vol. 39, no. 5, pp. 579–592, Sep. 1992.
[17] G. Lerosey, "Retournement temporel d'ondes électromagnétiques et application à la télécommunication en milieux complexes," Ph.D. dissertation, Univ. Paris 7 Denis Diderot, Paris, France, Dec. 2006.
[18] S. W. Mahfoud and D. E. Goldberg, "Parallel recombinative simulated annealing: A genetic algorithm," *Parallel Comput.*, vol. 21, no. 1, pp. 1–28, 1995.
[19] R. W. Eglese, "Simulated annealing: A tool for operational research," *Eur. J. Oper. Res.*, vol. 46, no. 3, pp. 271–281, 1990.
[20] J. B. Allen and D. A. Berkley, "Image method for efficiently simulating small-room acoustics," *J. Acoust. Soc. Amer.*, vol. 65, pp. 943–950, Apr. 1979.
[21] *Visaton—Lautsprecher und Zubehör, Loudspeakers and Accessories, SC 8 N 8 Ohm*, VISATON, Germany, 2008.
[22] I. Rishabh, D. Kimber, and J. Adcock, "Indoor localization using controlled ambient sounds," in *Proc. Int. Conf. Indoor Positioning Indoor Navigat.*, Sydney, NSW, Australia, Nov. 2012, pp. 1–10.

Nadia Aloui received the Engineering degree in telecommunications and the M.Sc degree in communication systems from the National Engineering School of Tunis, Tunisia, in 2009 and 2010, respectively, and the Ph.D. degree in signal image parole telecom from the University of Grenoble Alpes, France, and the University of Tunis El Manar, Tunisia, in 2014.

She was with the Gipsa-Laboratory, University of Grenoble Alpes, France, and the Sys'Com Laboratory, University Tunis El Manar, Tunisia, during her Ph.D. studies. From 2011 to 2012, she was a University Assistant at the Higher School of e-Commerce of Tunis. Her research interests include indoor localization, signal processing, joint source-channel coding, and digital communications.

Kosai Raoof received the M.Sc. and Ph.D. degrees from Grenoble University, in 1990 and 1993, respectively, the Habilitation à Diriger Des Recherches Degree in 1998. He is currently the Head of the Real Time Embeded Systems Department with the ENSIM College of Engineering, University of Maine, Le Mans, France. He was invited to join Laboratoire des Images et Signaux in 1999, to participate in the founding of telecommunication research group. His research interest was first focalized on advanced MIMO systems and joint CDMA synchronization; he studied and introduced polarized diversity MIMO systems in the research group. In 2007, he joined the Gipsa-Laboratory to continue his research on MIMO antenna selection systems. Since 2011, he has been a Full Professor with the University of Maine, and establishes a new group of research on signal processing and instrumentation at the LAUM Laboratory.

Ammar Bouallegue was born in Tunis, Tunisia, in 1945. He received the Electrical Engineering and Engineer-Doctor degrees from ENSERG, Grenoble, France, in 1971 and 1976, respectively, and the Ph.D. degree from ENSEEIHT, INP of Toulouse, France, in 1984. In 1976, he joined the Engineering School of Tunis (ENIT), Tunisia. From 1984 to 1992, he was the Head of the Electrical Department, ENIT, and from 1993 to 1995, he was the Director of Telecommunication with the High School of Tunis, Tunisia. He was the Head of the Communication Systems (Sys'Com) Laboratory with the Engineering School of Tunis till 2012. Since 2012, he has been a Professor Emeritus. His research interests include passive and active microwave structures, signal coding theory, and digital communications.

Stéphane Letourneur received the Instrumentation and Measurement Engineering degree from CNAM, Paris, in 2007. He is currently a CNRS Research Engineer with the LAUM Laboratory, Le Mans, France. His research interests are acoustic measurement techniques, especially with ultrasound.

Sonia Zaibi was born in Tunis, Tunisia, in 1974. She received the (Hons.) degree in telecommunications engineering from the National School of Engineers of Tunis, in 1999, and the M.Sc. and Ph.D. degrees in electronic engineering from the University of Bretagne Occidentale, Brest, France, in 2000 and 2004, respectively. During her M.Sc. and Ph.D. studies, she was with the Department of Signal and Communications, Telecom Bretagne, Brest, France. Since 2004, she has been with the National School of Engineers of Tunis, where she is currently an Assistant Professor and a member of the Sys'Com Laboratory. Her research interests include information theory, joint source-channel coding, error control coding, data compression, and digital communications.